



Results with a Locally Refined MAC-Like Scheme - Benchmark Session

Eric Chénier, Robert Eymard, Raphaele Herbin

► To cite this version:

Eric Chénier, Robert Eymard, Raphaele Herbin. Results with a Locally Refined MAC-Like Scheme - Benchmark Session. Finite Volumes for Complex Applications 8, Jun 2017, Lille, France. pp.2182 - 139. hal-01546509

HAL Id: hal-01546509

<https://hal.science/hal-01546509>

Submitted on 24 Jun 2017

HAL is a multi-disciplinary open access archive for the deposit and dissemination of scientific research documents, whether they are published or not. The documents may come from teaching and research institutions in France or abroad, or from public or private research centers.

L'archive ouverte pluridisciplinaire **HAL**, est destinée au dépôt et à la diffusion de documents scientifiques de niveau recherche, publiés ou non, émanant des établissements d'enseignement et de recherche français ou étrangers, des laboratoires publics ou privés.

Results with a locally refined MAC-like scheme – benchmark session

Eric Chénier, Robert Eymard and Raphaële Herbin

Abstract We recall the extension of the Marker and Cell (MAC) scheme for locally refined grids which was introduced in [3] and present the results obtained on the lid driven cavity test.

Key words: MAC scheme, locally refined meshes

MSC (2010): 65M08, 65N08, 35Q30

1 An extension of the MAC scheme on generalized meshes

The well known Marker-and-Cell (MAC) scheme [6] was originally designed on conforming rectangular meshes. An extension of the MAC scheme was proposed in [4] to deal with non-conforming rectangular meshes with hanging nodes, which include locally refined meshes. We test here the resulting scheme, which we shall denote by LR-MAC scheme in the sequel, on the lid-cavity test with a corner refinement. Let us first recall the general principle of the LR-MAC scheme. Let Ω be an

Eric Chénier
Université Paris-Est Marne-la-Vallée, laboratoire Modélisation et Simulation Multi-Echelle, UMR 8208 CNRS,
F-77454 Marne-la-Vallee, France
e-mail: eric.chenier@u-pem.fr

Robert Eymard
Université Paris-Est Marne-la-Vallée, Laboratoire d'Analyse et de Mathématiques Appliquées,
UPEC, UPEM, UMR8050 CNRS,
F-77454, Marne-la-Vallée, France
e-mail: robert.eymard@u-pem.fr

Raphaële Herbin
Aix Marseille Univ, CNRS, Centrale Marseille, I2M, Marseille, France
e-mail: raphael.eherbin@univ-amu.fr

open bounded set of \mathbb{R}^d . The weak formulation of the steady-state Navier-Stokes equations with homogeneous Dirichlet boundary conditions posed on Ω reads:

$$\begin{cases} \mathbf{u} = (u^{(i)})_{i=1,\dots,d} \in H_0^1(\Omega)^d, \operatorname{div} \mathbf{u} = 0 \text{ a.e. in } \Omega, \\ p \in L^2(\Omega) \text{ with } \int_{\Omega} p(\mathbf{x}) d\mathbf{x} = 0, \\ v \int_{\Omega} \nabla \mathbf{u}(\mathbf{x}) : \nabla \mathbf{v}(\mathbf{x}) d\mathbf{x} + \chi \int_{\Omega} (\mathbf{u}(\mathbf{x}) \cdot \nabla) \mathbf{u}(\mathbf{x}) \cdot \mathbf{v}(\mathbf{x}) d\mathbf{x} \\ \quad - \int_{\Omega} p(\mathbf{x}) \operatorname{div} \mathbf{v}(\mathbf{x}) d\mathbf{x} = \int_{\Omega} \mathbf{f}(\mathbf{x}) \cdot \mathbf{v}(\mathbf{x}) d\mathbf{x}, \forall \mathbf{v} \in H_0^1(\Omega)^d, \end{cases} \quad (1)$$

where $\mathbf{u} = (u^{(i)})_{i=1,\dots,d}$ is the velocity of the fluid, $v > 0$ its viscosity, $\mathbf{f} \in L^2(\Omega)$ some forcing term and where $\nabla \mathbf{u}(\mathbf{x}) : \nabla \mathbf{v}(\mathbf{x}) = \sum_{i=1}^d \nabla u^{(i)}(\mathbf{x}) \cdot \nabla v^{(i)}(\mathbf{x})$ for a.e. $\mathbf{x} \in \Omega$, and all $\mathbf{u}, \mathbf{v} \in H_0^1(\Omega)^d$. The coefficient χ is strictly positive in the general (nonlinear) case and is set to 0 to obtain the linear Stokes problem.

We consider a mesh of Ω denoted by \mathcal{M} , called the pressure mesh, such that all internal edges (2D) or faces (3D) (from now on, we only use the word “face”, in 2D or 3D) have their normal vector parallel to one of the basis vector $\mathbf{e}^{(k)}$ of the space \mathbb{R}^d , for some $k = 1, \dots, d$. In other words, all internal edges must be orthogonal to one of the reference axes. Note that on the other hand, the external faces, that is the faces of the mesh lying on the boundary $\partial\Omega$ need not be orthogonal to one of the reference axes: they are only assumed to be planar. So domains with tilted boundaries may be meshed with such grids, and in the case of curved boundaries, it is possible to use local refinement close to the boundaries (see [3]). Note that the locally refined meshes of the FVCA8 benchmark satisfy the above constraint on the internal faces as shown in Figure 1, which provides an example of pressure mesh (black lines in left or right figures).

For all $K \in \mathcal{M}$, we denote by \mathcal{E}_K the set of all internal faces of K (therefore, the faces of K which are on $\partial\Omega$ are not elements of \mathcal{E}_K), and we define the set \mathcal{E} as the union over $K \in \mathcal{M}$ of all the sets \mathcal{E}_K . It is assumed that a given interior edge σ is entirely included in an interface between two cells, say K and L ; we shall write $\sigma \in K|L$. Note that $K|L$ is allowed to contain several faces of the mesh; this may for instance happen in adaptive mesh refinement (and de-refinement) procedures. We then introduce the set $\mathcal{E}^{(k)}$ as the subset of \mathcal{E} which contains all the internal faces whose normal is parallel to the basis vector $\mathbf{e}^{(k)}$. For any $\sigma \in \mathcal{E}$, \mathbf{x}_{σ} denotes the center of gravity of σ .

In order to get a discrete variational MAC-like scheme, we consider, for any $k = 1, \dots, d$, the set of internal points $\mathcal{V}_{\text{int}}^{(k)} = (\mathbf{x}_{\sigma})_{\sigma \in \mathcal{E}^{(k)}}$ and a given family of external points $\mathcal{V}_{\text{ext}}^{(k)}$ containing at least all the vertices of Ω .

The diffusion term is discretized by a linear finite element approximation. To this purpose, we introduce a Delaunay triangulation $\mathcal{T}^{(k)}$ of Ω whose vertices are $\mathcal{V}_{\text{int}}^{(k)} \cup \mathcal{V}_{\text{ext}}^{(k)}$. Such a triangulation of Ω is a set of simplices: triangles in 2D, tetrahedra in 3D. Each simplex has $d+1$ vertices which belong to $\mathcal{V}_{\text{int}}^{(k)} \cup \mathcal{V}_{\text{ext}}^{(k)}$. The triangulation is assumed to satisfy the Delaunay property, which means that the in-

terior of the circumcircle (in 2D) or of the circumsphere (in 3D) of any simplex $T \in \mathcal{T}^{(k)}$ does not contain any element of $\mathcal{V}_{\text{int}}^{(k)} \cup \mathcal{V}_{\text{ext}}^{(k)}$. Examples of Delaunay triangulations constructed from the edge mid-points are illustrated in Figure 1 (left part for the horizontal velocity, right part for the vertical velocity).

We then denote, for any $\sigma \in \mathcal{E}^{(k)}$, the function $\xi_{\sigma}^{(k)}$, which is continuous, piecewise P^1 on any $T \in \mathcal{T}^{(k)}$, and whose value is 1 at the point \mathbf{x}_{σ} and 0 at points $\mathbf{x}_{\sigma'}$ for any $\sigma' \in \mathcal{E}^{(k)} \setminus \{\sigma\}$.

Let $\{V_{\sigma}^{(k)}, \sigma \in \mathcal{E}^{(k)}\}$ be the Voronoï mesh associated to the family $(\mathbf{x}_{\sigma})_{\sigma \in \mathcal{E}^{(k)}}$, defining the Voronoï cells as follows:

$$V_{\sigma}^{(k)} = \{\mathbf{x} \in \Omega, d(\mathbf{x}, \mathbf{x}_{\sigma}) < d(\mathbf{x}, \mathbf{x}_{\sigma'}), \sigma' \in \mathcal{E}^{(k)} \setminus \{\sigma\}\}, \forall \sigma \in \mathcal{E}^{(k)}.$$

The Voronoï mesh construction in the case of the pressure and Delaunay meshes shown in Figure 1 is shown in Figure 2. Note that the Voronoï cells $V_{\sigma}^{(k)}$ shown in this figure do not all satisfy $V_{\sigma}^{(k)} \subset \Omega$. This does not prevent from the convergence of the scheme since this only introduces a vanishing error in the nonlinear convection term defined below. We finally denote by \mathcal{D} the collection of all the space discretization data.

We define $H_{\mathcal{M}}(\Omega)$ as the set of piecewise functions constant on the pressure cells $K \in \mathcal{M}$, the set $H_{\mathcal{E}}^{(k)}(\Omega)$ of piecewise constant functions on the dual grid cells V_{σ} , for $\sigma \in \mathcal{E}^{(k)}$; this discrete set is the space of functions meant to approximate the k -th component of the velocity. We then denote by $\mathbf{H}_{\mathcal{E}}(\Omega)$ the set of all $\mathbf{v} = (v^{(k)})_{k=1,\dots,d}$ with $v^{(k)} \in H_{\mathcal{E}}^{(k)}(\Omega)$. We then define:

$$\hat{v}^{(k)} = \sum_{\sigma \in \mathcal{E}^{(k)}} v_{\sigma} \xi_{\sigma}^{(k)} \in H_0^1(\Omega), \quad (2)$$

we denote by $\hat{\mathbf{v}} = (\hat{v}^{(k)})_{k=1,\dots,d}$, and we define the norm

$$\|\mathbf{v}\|_{\mathcal{E}} = \|\nabla \hat{\mathbf{v}}\|_{L^2(\Omega)^{d \times d}}, \forall \mathbf{v} \in \mathbf{H}_{\mathcal{E}}(\Omega). \quad (3)$$

The piecewise constant discrete divergence of $\mathbf{v} \in \mathbf{H}_{\mathcal{E}}(\Omega)$ is the function $\text{div}_{\mathcal{M}} \mathbf{v} \in H_{\mathcal{M}}(\Omega)$ defined by:

$$\forall K \in \mathcal{M}, \forall \mathbf{v} \in \mathbf{H}_{\mathcal{E}}(\Omega),$$

$$\text{div}_{\mathcal{M}} \mathbf{v}(\mathbf{x}) = \text{div}_K \mathbf{v} = \frac{1}{|K|} \sum_{k=1}^d \sum_{\sigma \in \mathcal{E}_K} |\sigma| v_{K,\sigma}, \text{ for a.e. } \mathbf{x} \in K,$$

where $v_{K,\sigma} = v_{\sigma} \mathbf{n}_{K,\sigma} \cdot \mathbf{e}^{(k)}$. (4)

In order to complete the scheme for the Navier-Stokes equations, we need to give a discretization of the nonlinear term $b(\mathbf{u}, \mathbf{v}, \mathbf{w}) = \int_{\Omega} (\mathbf{u}(\mathbf{x}) \cdot \nabla) \mathbf{u}(\mathbf{x}) \cdot \mathbf{v}(\mathbf{x}) d\mathbf{x}$. To this purpose, we introduce a discrete trilinear form $b_{\mathcal{E}}$ defined on $(H_{\mathcal{M}}(\Omega))^d$. We

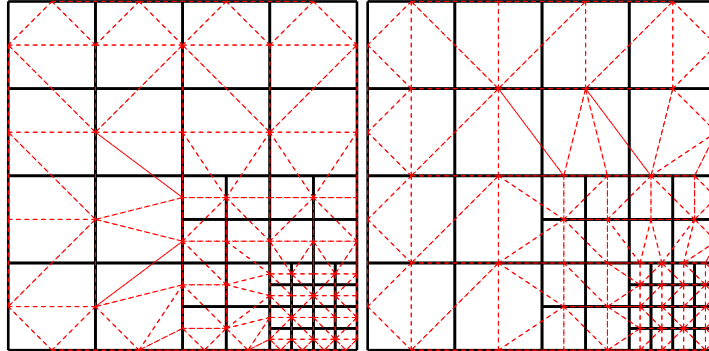


Fig. 1 Pressure and velocity grids (left: horizontal velocity, right: vertical velocity).

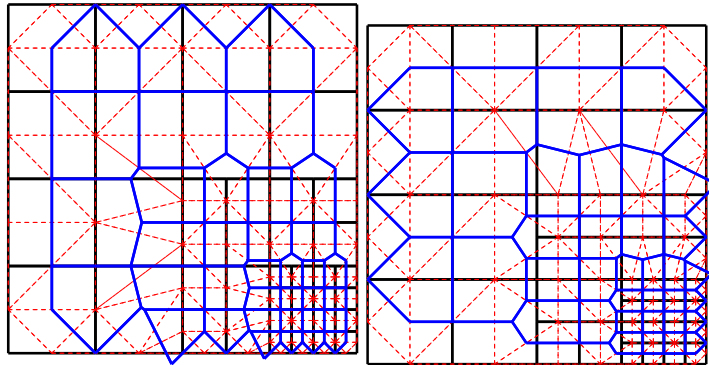


Fig. 2 The Delaunay triangulation and the Voronoi cells (left: horizontal velocity, right: vertical velocity).

begin by defining some interpolation operators between $\mathbf{H}_{\mathcal{E}}(\Omega)$ and $(H_{\mathcal{M}}(\Omega))^d$. For $\mathbf{v} \in \mathbf{H}_{\mathcal{E}}(\Omega)$, we define $\boldsymbol{\Pi}_K \mathbf{v}$ by its components $(\boldsymbol{\Pi}_K \mathbf{v})^{(k)}$:

$$(\boldsymbol{\Pi}_K \mathbf{v})^{(k)} = \frac{1}{\sum_{\sigma \in \mathcal{E}_K^{(k)}} |\sigma|} \sum_{\sigma \in \mathcal{E}_K^{(k)}} |\sigma| v_{\sigma}, k = 1, \dots, d, \quad (5)$$

and $\boldsymbol{\Pi}_{\mathcal{M}} \mathbf{v} \in \mathbf{H}_{\mathcal{M}}(\Omega) = (H_{\mathcal{M}}(\Omega))^d$ as the piecewise constant function equal to $(\boldsymbol{\Pi}_K \mathbf{v})$ on each cell K . We then define $\boldsymbol{\Pi}_{\mathcal{E}} \mathbf{v} \in \mathbf{H}_{\mathcal{E}}(\Omega)$ as the following piecewise constant function on the Voronoi cells:

$$\boldsymbol{\Pi}_{\mathcal{E}} \mathbf{w} = \sum_{\substack{\sigma \in \mathcal{E}_{\text{int}} \\ \sigma \in K | L}} \frac{1}{2} (\boldsymbol{\Pi}_K \mathbf{w} + \boldsymbol{\Pi}_L \mathbf{w}) \mathbf{1}_{V_{\sigma}},$$

where $\mathbf{1}_{V_{\sigma}}$ denotes the characteristic function of V_{σ} , that is $\mathbf{1}_{V_{\sigma}}(\mathbf{x}) = 1$ if $\mathbf{x} \in V_{\sigma}$ and 0 otherwise. For $v \in H_{\mathcal{M}}(\Omega)$, we define its discrete gradient $\nabla_{\mathcal{E}} v \in \mathbf{H}_{\mathcal{E}}(\Omega)$ by:

$$\nabla_{\mathcal{E}} v = \left(\partial_{\mathcal{E}}^{(1)} v, \dots, \partial_{\mathcal{E}}^{(d)} v \right)^t, \text{ with } \partial_{\mathcal{E}}^{(i)} v = \sum_{\sigma \in \mathcal{E}^{(i)}} \partial_{\sigma} v \mathbf{1}_{V_{\sigma}}$$

$$\text{and } \partial_{\sigma} v = \begin{cases} (v_L - v_K) \frac{|\sigma|}{|V_{\sigma}|}, & \text{if } \sigma \in \mathcal{E}_{\text{int}}, \sigma \in \overrightarrow{K|L}, \\ 0, & \text{if } \sigma \in \mathcal{E}_{\text{ext}}, \end{cases} \quad (6)$$

where $\sigma \in \overrightarrow{K|L}$ means that $\sigma \in K|L \subset \mathcal{E}^{(k)}$ for some $k = 1, \dots, d$ and $\mathbf{n}_{K,\sigma} \cdot \mathbf{e}^{(k)} = 1$.

With these definitions, the following discrete duality properties hold:

$$\begin{aligned} \forall p \in H_{\mathcal{M}}, \forall \mathbf{v} \in (H_0^1(\Omega))^d, \int_{\Omega} p(\mathbf{x}) \operatorname{div}_{\mathcal{M}} P_{\mathcal{E}} \mathbf{v}(\mathbf{x}) d\mathbf{x} &= \int_{\Omega} p(\mathbf{x}) \operatorname{div} \mathbf{v}(\mathbf{x}) d\mathbf{x}, \\ \forall \mathbf{u} \in \mathbf{H}_{\mathcal{E}}, \forall q \in H_{\mathcal{M}}(\Omega), \int_{\Omega} q(\mathbf{x}) \operatorname{div}_{\mathcal{M}} \mathbf{u} d\mathbf{x} &= - \int_{\Omega} \nabla_{\mathcal{E}} q(\mathbf{x}) \cdot \mathbf{u}(\mathbf{x}) d\mathbf{x}. \end{aligned}$$

We then define the following trilinear form $b_{\mathcal{E}}$ on $(\mathbf{H}_{\mathcal{E}}(\Omega))^3$ by:

$$b_{\mathcal{E}}(\mathbf{u}, \mathbf{v}, \mathbf{w}) = \int_{\Omega} (\mathbf{u} \cdot \nabla_{\mathcal{E}}) \boldsymbol{\Pi}_{\mathcal{M}} \mathbf{v} \cdot \boldsymbol{\Pi}_{\mathcal{E}} \mathbf{w} d\mathbf{x}, \text{ for } \mathbf{u}, \mathbf{v}, \mathbf{w} \in \mathbf{H}_{\mathcal{E}}(\Omega) \quad (7)$$

where, for any $\tilde{\mathbf{v}} \in \mathbf{H}_{\mathcal{M}}(\Omega)$,

$$(\mathbf{u} \cdot \nabla_{\mathcal{E}}) \tilde{\mathbf{v}}(\mathbf{x}) = \sum_{i=1}^d \sum_{\sigma \in \mathcal{E}^{(i)}} u_{\sigma} \partial_{\sigma} \tilde{\mathbf{v}} \mathbf{1}_{V_{\sigma}}(\mathbf{x}).$$

In particular, the trilinear form $b_{\mathcal{E}}$ thus defined satisfies $b_{\mathcal{E}}(\mathbf{u}, \mathbf{v}, \mathbf{w}) = 0$ for any $\mathbf{u}, \mathbf{v} \in \mathbf{H}_{\mathcal{M}}(\Omega)$ s.t. $\operatorname{div}_{\mathcal{M}} \mathbf{u} = 0$.

The LR-MAC scheme for the Navier-Stokes equation (1) then reads:

Find $\mathbf{u} \in \mathbf{H}_{\mathcal{E}}(\Omega)$ and $p \in H_{\mathcal{M}}(\Omega)$ s. t.

$$\sum_{K \in \mathcal{M}} |K| p_K = 0, \quad (8a)$$

$$\operatorname{div}_{\mathcal{M}} \mathbf{u}(\mathbf{x}) = 0, \text{ for a.e. } \mathbf{x} \in \Omega. \quad (8b)$$

$$\begin{aligned} \nu \int_{\Omega} \nabla \mathbf{u}(\mathbf{x}) : \nabla \mathbf{v}(\mathbf{x}) d\mathbf{x} - \int_{\Omega} p(\mathbf{x}) \operatorname{div}_{\mathcal{M}} \mathbf{v}(\mathbf{x}) d\mathbf{x} + \chi b_{\mathcal{E}}(\mathbf{u}, \mathbf{u}, \mathbf{v}) \\ = \int_{\Omega} \mathbf{f}(\mathbf{x}) \cdot \mathbf{v}(\mathbf{x}) d\mathbf{x}, \forall \mathbf{v} \in \mathbf{H}_{\mathcal{E}}(\Omega). \end{aligned} \quad (8c)$$

Note that the scheme (8) is strictly equivalent to the classical MAC scheme in the case of the (linear) Stokes equations and a regular Cartesian grid. In the case of the Navier-Stokes equations, however, the nonlinear convective term has a stencil which is wider than the classical MAC scheme, whose convergence is proved in [5]; a version of this latter scheme for locally refined meshes using a multi-point flux approximation scheme for the Laplace operator is available in the software CALIF³S [1] developed at IRSN.

2 Numerical results on the lid driven cavity benchmark test

2.1 General comments on the results

We now give the results obtained with the LR-MAC scheme described above in the case of the lid driven cavity test of the FVCA8 benchmark, considering the meshes of the family “mesh_ref” (the coarsest one is shown in Figure 1). Here we rely on the fact that the LR-MAC scheme can handle this case with hanging nodes (this is not directly the case for the standard MAC scheme, nor for standard finite element schemes). Note however that there are several schemes for the Stokes and Navier-Stokes problems which are not directly suited to such meshes but which can nevertheless be applied on conforming submeshes of the initial mesh, so that it is difficult to exhibit a clear criterion stating whether a scheme can be used on a given grid. We nevertheless observe that the LR-MAC scheme directly provides the mass fluxes on the initial refined mesh, since these fluxes are exactly the discrete unknowns of the scheme, together with the pressure in each cell of the initial mesh, so we guess that the LR-MAC scheme may be one of those showing the lowest number of unknowns on a grid of this type.

In our implementation, the nonlinear system is solved using the Newton method (using under-relaxation as long as the solution is far from convergence), without any optimization procedure, using LU factorization for the resulting linear systems. The number of iterations is of order 10 for the coarsest mesh and 20 for the finest mesh. In Table 1, we provide some indication of the complexity of the computations:

1. in the first column, we precise the mesh used,
2. in column “nuu”, we give the number of velocity unknowns,
3. in column “npu”, we give the number of pressure unknowns,
4. in column “nlm”, we give the total number of unknowns,
5. in column “nnzut”, we give the number of nonzero entries of the Jacobian matrix,
6. in column “nnzutresol”, we give the number of nonzero entries of the LU factorization of the Jacobian matrix.

mesh	nuu	npu	nlm = nuu + npu	nnzut	nnzutresol
ref1	72	40	112	1 558	2 732
ref2	304	160	464	6 949	24 686
ref3	1 248	640	1 888	29 250	208 254
ref4	5 056	2 560	7 616	119 785	1 704 422
ref5	20 352	10 240	30 592	484 599	13 774 257
ref6	81 664	40 960	122 624	1 954 372	110 960 777
ref7	327 168	163 840	491 008	7 841 053	887 641 033

Table 1 Complexity table on locally refined meshes.

2.2 Case $\nu = 1/100$

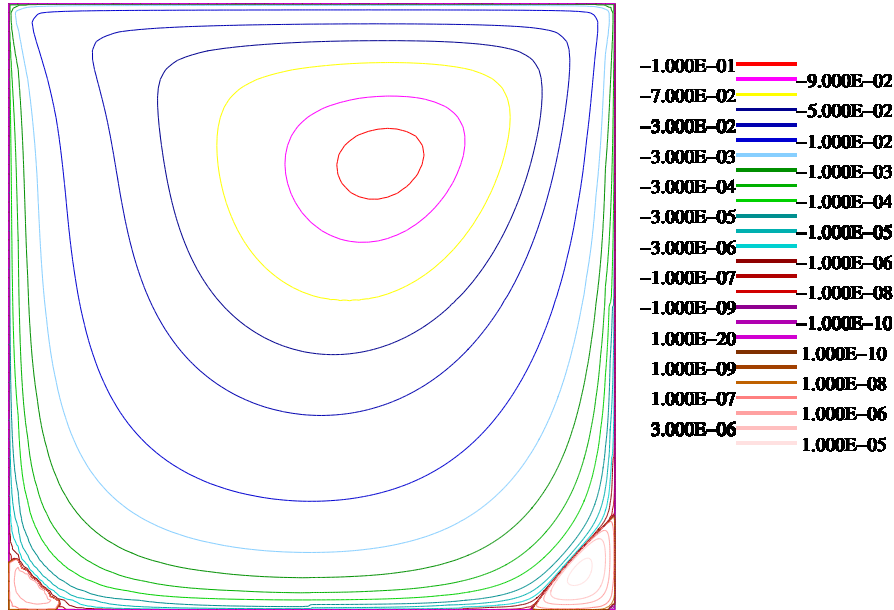


Fig. 3 Streamlines for $\nu = 1/100$ (mesh_5)

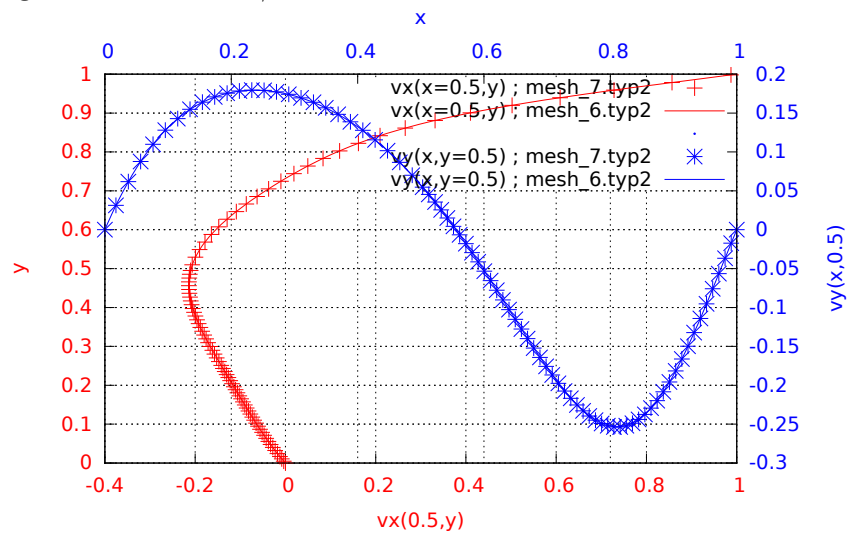


Fig. 4 Velocity profiles for $\nu = 1/100$

We observe that for the case $\nu = 1/100$, the convergence seems to be achieved with the finest grid.

mesh #	x_{\min}	y_{\min}	ψ_{\min}	x_{\max}	y_{\max}	ψ_{\max}
1	0.500	0.750	$-8.368 \cdot 10^{-2}$	0.938	$6.25 \cdot 10^{-2}$	$3.774 \cdot 10^{-5}$
2	0.625	0.750	$-9.273 \cdot 10^{-2}$	0.938	$6.25 \cdot 10^{-2}$	$1.537 \cdot 10^{-5}$
3	0.625	0.750	$-9.899 \cdot 10^{-2}$	$6.25 \cdot 10^{-2}$	$6.25 \cdot 10^{-2}$	$1.564 \cdot 10^{-5}$
4	0.625	0.750	-0.102	0.945	$6.25 \cdot 10^{-2}$	$1.249 \cdot 10^{-5}$
5	0.609	0.734	-0.103	0.941	$6.25 \cdot 10^{-2}$	$1.259 \cdot 10^{-5}$
6	0.609	0.617	-0.103	0.943	$6.25 \cdot 10^{-2}$	$1.269 \cdot 10^{-5}$
7	0.617	0.738	-0.103	0.942	$6.152 \cdot 10^{-2}$	$1.272 \cdot 10^{-5}$

Table 2 Stream function table : Lid driven cavity - Locally refined meshes - $\nu = 1/100$

Mesh #	y	0.0000	0.0625	0.1016	0.2813	0.5000	0.7344	0.9531	0.9688	1.0000
1	0.0000	-0.0538	-0.0722	-0.1408	-0.1274	0.0858	0.7504	0.8339	1.0000	
2	0.0000	-0.0410	-0.0626	-0.1407	-0.1617	0.0074	0.6644	0.7767	1.0000	
3	0.0000	-0.0396	-0.0606	-0.1457	-0.1907	-0.0053	0.6843	0.7737	1.0000	
4	0.0000	-0.0413	-0.0634	-0.1541	-0.2038	0.0001	0.6862	0.7909	1.0000	
5	0.0000	-0.0419	-0.0642	-0.1568	-0.2077	0.0033	0.6908	0.7917	1.0000	
6	0.0000	-0.0420	-0.0644	-0.1575	-0.2088	0.0040	0.6910	0.7919	1.0000	
7	0.0000	-0.0420	-0.0644	-0.1576	-0.2090	0.0041	0.6910	0.7919	1.0000	

Table 3 Hor. velocity $y \mapsto u(0.5, y)$: Lid driven cavity - Locally refined meshes - $\nu = 1/100$

Mesh #	x	0.0000	0.0703	0.0938	0.2266	0.5000	0.8594	0.9453	0.9609	1.0000
1	0.0000	0.0683	0.0912	0.1149	0.0083	-0.1655	-0.1032	-0.10738	0.0000	
2	0.0000	0.0864	0.0978	0.1427	0.0487	-0.2049	-0.1334	-0.1096	0.0000	
3	0.0000	0.0916	0.1157	0.1629	0.0518	-0.2226	-0.1074	-0.0773	0.0000	
4	0.0000	0.1004	0.1224	0.1746	0.0554	-0.2296	-0.1075	-0.0781	0.0000	
5	0.0000	0.1031	0.1255	0.1783	0.0570	-0.2327	-0.1084	-0.0779	0.0000	
6	0.0000	0.1034	0.1262	0.1791	0.0574	-0.2335	-0.1085	-0.0780	0.0000	
7	0.0000	0.1035	0.1264	0.1793	0.0575	-0.2336	-0.1085	-0.0780	0.0000	

Table 4 Ver. velocity $x \mapsto v(x, 0.5)$: Lid driven cavity - Locally refined meshes - $\nu = 1/100$

2.3 Case $\nu = 1/400$

We observe that for the case $\nu = 1/400$, the convergence seems to be achieved with the finest grid.

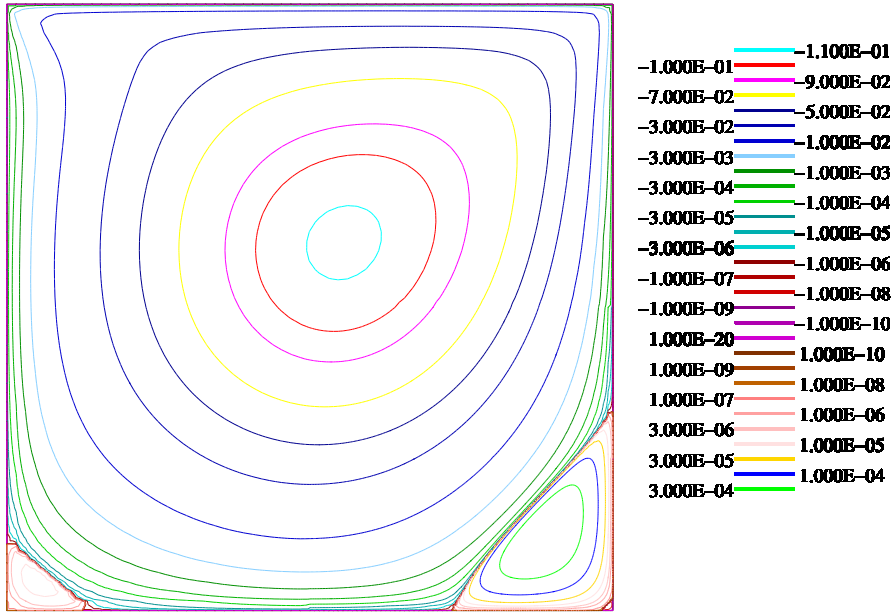


Fig. 5 Streamlines for $v = 1/400$ (mesh_5)

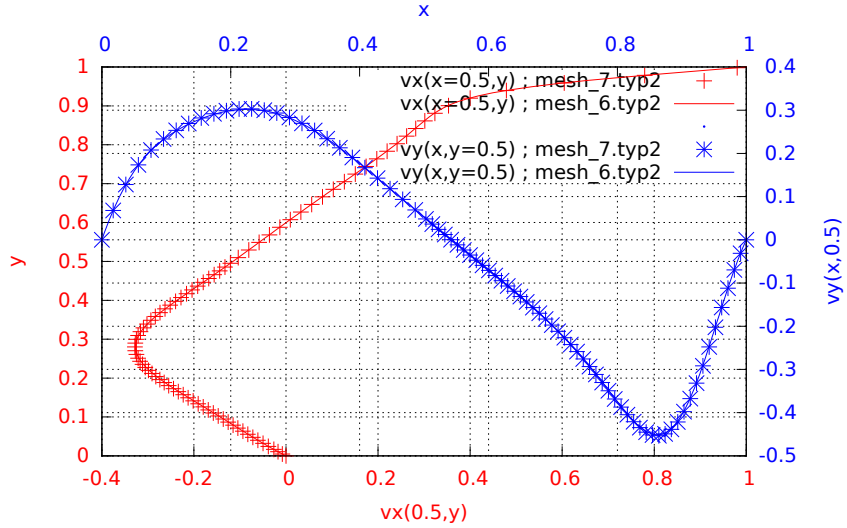


Fig. 6 Velocity profiles for $v = 1/400$

2.4 Case $v = 1/1000$

We observe that for the case $v = 1/1000$, the convergence seems to be achieved with the finest grid, which is confirmed by the very good agreement with the literature [2], both for the extreme stream values and the velocity profiles along the midlines.

mesh #	x_{\min}	y_{\min}	ψ_{\min}	x_{\max}	y_{\max}	ψ_{\max}
1	0.500	0.750	$-6.762 \cdot 10^{-2}$	0.938	0.188	$4.425 \cdot 10^{-4}$
2	0.625	0.625	$-8.287 \cdot 10^{-2}$	0.938	$6.25 \cdot 10^{-2}$	$7.276 \cdot 10^{-5}$
3	0.563	0.625	$-9.625 \cdot 10^{-2}$	0.891	0.125	$4.22 \cdot 10^{-4}$
4	0.563	0.625	-0.107	0.883	0.125	$5.895 \cdot 10^{-4}$
5	0.563	0.609	-0.112	0.887	0.125	$5.895 \cdot 10^{-4}$
6	0.555	0.609	-0.114	0.887	0.123	$6.397 \cdot 10^{-4}$
7	0.555	0.605	-0.114	0.886	0.122	$6.432 \cdot 10^{-4}$

Table 5 Stream function table : Lid driven cavity - Locally refined meshes - $\nu = 1/400$

Mesh #	y	0.0000	0.0625	0.1016	0.2813	0.5000	0.7344	0.9531	0.9688	1.0000
1	0.0000	-0.0789	-0.0967	-0.1507	-0.0598	0.0881	0.7263	0.8179	1.0000	
2	0.0000	-0.0875	-0.1322	-0.2194	-0.0722	0.1080	0.5509	0.7012	1.0000	
3	0.0000	-0.0681	-0.1075	-0.2510	-0.1178	0.1302	0.5392	0.6189	1.0000	
4	0.0000	-0.0799	-0.1266	-0.3000	-0.1195	0.1494	0.5345	0.6782	1.0000	
5	0.0000	-0.0895	-0.1413	-0.3211	-0.1158	0.1589	0.5583	0.6844	1.0000	
6	0.0000	-0.0918	-0.1450	-0.3268	-0.1152	0.1616	0.5608	0.6865	1.0000	
7	0.0000	-0.0924	-0.1459	-0.3282	-0.1151	0.1623	0.5614	0.6871	1.0000	

Table 6 Hor. velocity $y \mapsto u(0.5, y)$: Lid driven cavity - Locally refined meshes - $\nu = 1/400$

Mesh #	x	0.0000	0.0703	0.0938	0.2266	0.5000	0.8594	0.9453	0.9609	1.0000
1	0.0000	0.0562	0.0750	0.1068	0.0306	-0.1812	-0.0915	-0.0654	0.0000	
2	0.0000	0.1226	0.1342	0.1804	0.0624	-0.2731	-0.2555	-0.2187	0.0000	
3	0.0000	0.1374	0.1681	0.2273	0.0650	-0.3402	-0.2385	-0.1840	0.0000	
4	0.0000	0.1755	0.2053	0.2747	0.0551	-0.4137	-0.2119	-0.1474	0.0000	
5	0.0000	0.1931	0.2246	0.2962	0.0528	-0.4428	-0.2292	-0.1571	0.0000	
6	0.0000	0.1972	0.2299	0.3018	0.0523	-0.4510	-0.2334	-0.1605	0.0000	
7	0.0000	0.1984	0.2313	0.3033	0.0521	-0.4531	-0.2344	-0.1613	0.0000	

Table 7 Ver. velocity $x \mapsto v(x, 0.5)$: Lid driven cavity - Locally refined meshes - $\nu = 1/400$

mesh #	x_{\min}	y_{\min}	ψ_{\min}	x_{\max}	y_{\max}	ψ_{\max}
1	0.750	0.750	$-5.546 \cdot 10^{-2}$	0.875	0.188	$4.645 \cdot 10^{-3}$
2	0.500	0.625	$-6.945 \cdot 10^{-2}$	0.938	0.188	$9.432 \cdot 10^{-4}$
3	0.563	0.563	$-8.933 \cdot 10^{-2}$	0.906	0.109	$6.659 \cdot 10^{-4}$
4	0.531	0.563	-0.104	0.867	0.117	$1.535 \cdot 10^{-3}$
5	0.531	0.563	-0.114	0.863	0.113	$1.657 \cdot 10^{-3}$
6	0.531	0.563	-0.118	0.863	0.111	$1.712 \cdot 10^{-3}$
7	0.531	0.566	-0.119	0.864	0.112	$1.725 \cdot 10^{-3}$

	x_{\min}	y_{\min}	ψ_{\min}	x_{\max}	y_{\max}	ψ_{\max}
[2]	0.53125	0.56543	-0.11892	0.86328	0.1123	$1.7292 \cdot 10^{-3}$

Table 8 Stream function table : Lid driven cavity - Locally refined meshes - $\nu = 1/1000$

2.5 Case $\nu = 1/5000$

We observe that for the case $\nu = 1/5000$, the convergence seems to be nearly achieved with the finest grid. Note also that the location of the points at which the

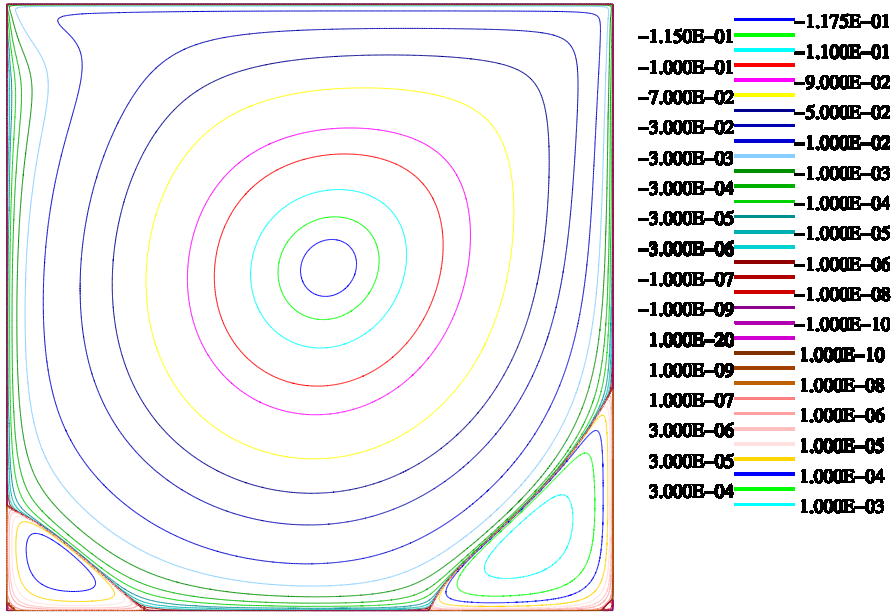


Fig. 7 Streamlines for $v = 1/1000$ (mesh_7)

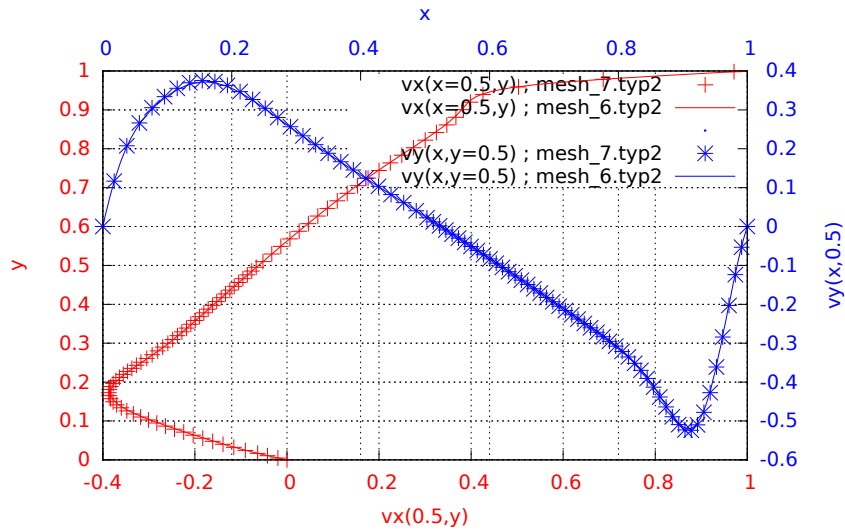


Fig. 8 Velocity profiles for $v = 1/1000$

extremum values are obtained is close to be converged, which is confirmed by the very good agreement with the literature [2].

Mesh #	y	0.0000	0.0625	0.1016	0.2813	0.5000	0.7344	0.9531	0.9688	1.0000
1	0.0000	-0.0923	-0.0987	-0.1200	-0.0119	0.0696	0.6968	0.7983	1.0000	
2	0.0000	-0.1540	-0.2176	-0.1768	-0.0245	0.1164	0.4824	0.6557	1.0000	
3	0.0000	-0.1618	-0.2213	-0.2139	-0.0434	0.1464	0.4294	0.4879	1.0000	
4	0.0000	-0.1535	-0.2308	-0.2614	-0.0611	0.1645	0.4148	0.5639	1.0000	
5	0.0000	-0.1880	-0.2793	-0.2736	-0.0612	0.1808	0.4590	0.5710	1.0000	
6	0.0000	-0.1984	-0.2948	-0.2786	-0.0618	0.1865	0.4686	0.5781	1.0000	
7	0.0000	-0.2013	-0.2990	-0.2799	-0.0620	0.1881	0.4714	0.5802	1.0000	
<i>y</i>	0.0000	0.0625	0.1016	0.2813	0.5000	0.7344	0.9531	0.9688	1.0000	
[2]	0.0000	-0.20227	-0.30029	-0.28040	-0.06205	0.18861	0.47239	0.58031	1.0000	

Table 9 Hor. velocity $y \mapsto u(0.5, y)$: Lid driven cavity - Locally refined meshes - $\nu = 1/1000$

Mesh #	x	0.0000	0.0703	0.0938	0.2266	0.5000	0.8594	0.9453	0.9609	1.0000
1	0.0000	0.0543	0.0724	0.0856	0.0223	-0.1449	-0.0384	-0.0274	0.0000	
2	0.0000	0.1515	0.1583	0.1735	0.0280	-0.2281	-0.2609	-0.2313	0.0000	
3	0.0000	0.1805	0.2126	0.2434	0.0365	-0.2754	-0.3803	-0.3526	0.0000	
4	0.0000	0.2367	0.2678	0.2921	0.0269	-0.3798	-0.3587	-0.2761	0.0000	
5	0.0000	0.2781	0.3123	0.3216	0.0259	-0.4140	-0.3903	-0.2773	0.0000	
6	0.0000	0.2911	0.3275	0.3306	0.0258	-0.4232	-0.4048	-0.2892	0.0000	
7	0.0000	0.2950	0.3316	0.3331	0.0258	-0.4256	-0.4089	-0.2925	0.0000	
<i>x</i>	0.0000	0.0703	0.0938	0.2266	0.5000	0.8594	0.9453	0.9609	1.0000	
[2]	0.0000	0.29622	0.33290	0.33398	0.02580	-0.42634	-0.41018	-0.29330	0.0000	

Table 10 Ver. velocity $x \mapsto v(x, 0.5)$: Lid driven cavity - Locally refined meshes - $\nu = 1/1000$

mesh #	x_{\min}	y_{\min}	ψ_{\min}	x_{\max}	y_{\max}	ψ_{\max}
1	0.750	0.750	$-2.454 \cdot 10^{-2}$	0.875	0.375	$7.521 \cdot 10^{-3}$
2	0.500	0.438	$-3.16 \cdot 10^{-2}$	0.938	0.219	$3.905 \cdot 10^{-3}$
3	0.563	0.563	$-6.533 \cdot 10^{-2}$	$6.25 \cdot 10^{-2}$	0.125	$6.008 \cdot 10^{-3}$
4	0.531	0.531	$-8.587 \cdot 10^{-2}$	$6.25 \cdot 10^{-2}$	0.188	$2.828 \cdot 10^{-3}$
5	0.516	0.531	-0.103	0.813	$7.813 \cdot 10^{-2}$	$2.847 \cdot 10^{-3}$
6	0.516	0.539	-0.116	0.807	$7.422 \cdot 10^{-2}$	$2.996 \cdot 10^{-3}$
7	0.516	0.535	-0.120	0.805	$7.324 \cdot 10^{-2}$	$3.054 \cdot 10^{-3}$
	x_{\min}	y_{\min}	ψ_{\min}	x_{\max}	y_{\max}	ψ_{\max}
[2]	0.51465	0.53516	-0.12191	0.80566	0.073242	$3.0694 \cdot 10^{-3}$

Table 11 Stream function table : Lid driven cavity - Locally refined meshes - $\nu = 1/5000$

3 Conclusion

Our results show that the LR-MAC scheme used here provides numerically converging results. An advantage of the LR-MAC scheme is its relatively small number of unknowns (as for a standard MAC scheme, only normal velocities at the faces of the pressure mesh and one pressure per cell are required).

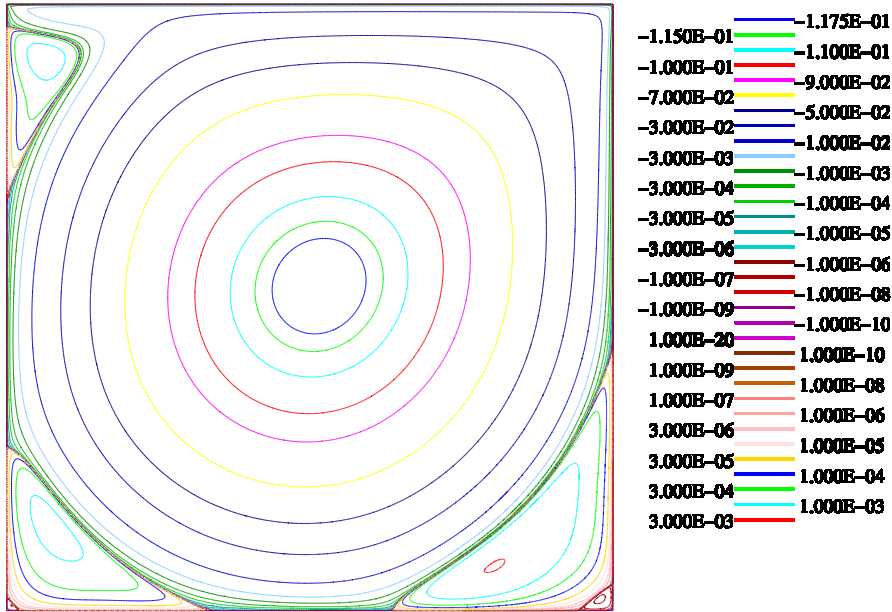


Fig. 9 Streamlines for $v = 1/5000$ (mesh_7)

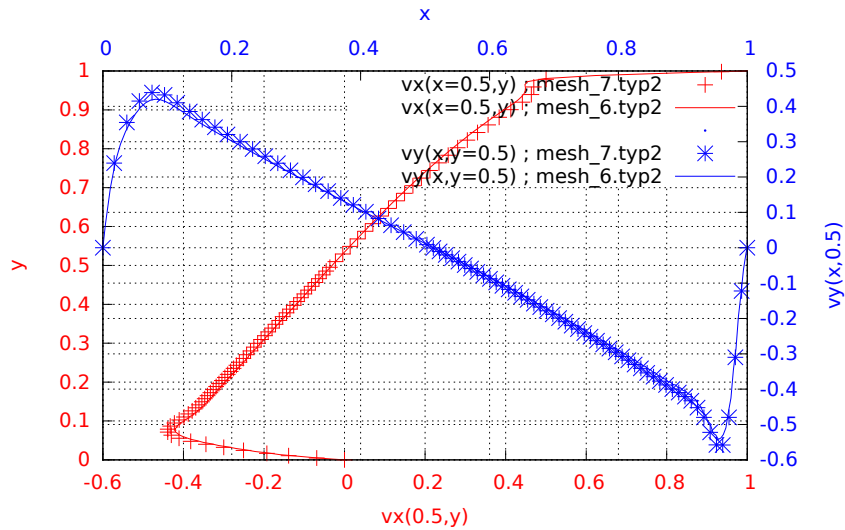


Fig. 10 Velocity profiles for $v = 1/5000$

References

1. CALIF³S. a software components library for the computation of reactive turbulent flows.
<https://gforge.irsn.fr/gf/project/isis>

Mesh #	y	0.0000	0.0625	0.1016	0.2813	0.5000	0.7344	0.9531	0.9688	1.0000
1	0.0000	-0.0343	-0.0384	-0.0662	0.0124	0.0237	0.6574	0.7721	1.0000	
2	0.0000	-0.1199	-0.1392	-0.0701	0.0421	0.0376	0.3564	0.5718	1.0000	
3	0.0000	-0.2699	-0.2078	-0.1208	-0.0103	0.1128	0.2773	0.3018	1.0000	
4	0.0000	-0.2978	-0.3098	-0.1655	-0.0206	0.1449	0.2955	0.3832	1.0000	
5	0.0000	-0.3447	-0.3551	-0.2025	-0.0289	0.1724	0.3916	0.4040	1.0000	
6	0.0000	-0.4067	-0.3970	-0.2247	-0.0308	0.1938	0.4491	0.4511	1.0000	
7	0.0000	-0.4281	-0.4114	-0.2329	-0.0317	0.2015	0.4701	0.4704	1.0000	

Table 12 Hor. velocity $y \mapsto u(0.5, y)$: Lid driven cavity - Locally refined meshes - $\nu = 1/5000$

Mesh #	x	0.0000	0.0703	0.0938	0.2266	0.5000	0.8594	0.9453	0.9609	1.0000
1	0.0000	0.0224	0.0299	0.0324	0.0264	-0.0616	0.0404	0.0289	0.0000	
2	0.0000	0.0771	0.0773	0.0716	-0.0097	-0.0884	-0.1265	-0.1107	0.0000	
3	0.0000	0.1871	0.2049	0.1579	0.0160	-0.1722	-0.3116	-0.3255	0.0000	
4	0.0000	0.2651	0.2801	0.2065	0.0199	-0.2532	-0.3685	-0.3708	0.0000	
5	0.0000	0.3547	0.3631	0.2468	0.0120	-0.3181	-0.4589	-0.4689	0.0000	
6	0.0000	0.4138	0.4158	0.2752	0.0117	-0.3575	-0.5144	-0.5334	0.0000	
7	0.0000	0.4353	0.4338	0.2854	0.0117	-0.3712	-0.5336	-0.5607	0.0000	

Table 13 Ver. velocity $x \mapsto v(x, 0.5)$: Lid driven cavity - Locally refined meshes - $\nu = 1/5000$

2. Bruneau, C.H., Saad, M.: The 2d lid-driven cavity problem revisited. *Computers & Fluids* **35**, 326–348 (2006)
3. Chénier, E., Eymard, R., Gallouët, T., Herbin, R.: An extension of the MAC scheme to locally refined meshes: convergence analysis for the full tensor time-dependent Navier-Stokes equations. *Calcolo* **52**(1), 69–107 (2015). DOI 10.1007/s10092-014-0108-x. URL <https://dx-doi.org.fennec.u-pem.fr/10.1007/s10092-014-0108-x>
4. Chénier, R., Eymard, R., Herbin, R.: An extension of the MAC scheme to some unstructured meshes. In: Finite volumes for complex applications VI, vol. 1, pp. 253–261. Springer, London (2011). *Finite Volumes for Complex Applications VI (FVCA VI)*, Prague, Czech Republic, June 2011
5. Gallouët, T., Herbin, R., Latché, J.C., Mallem, K.: Convergence of the MAC scheme for the incompressible Navier-Stokes equations. *Found Comput Math* (2016). URL <https://hal.archives-ouvertes.fr/hal-01189014>
6. Harlow, F., Welch, J.: Numerical calculation of time-dependent viscous incompressible flow of fluid with a free surface. *Physics of Fluids* **8**, 2182–2189 (1965)